Soil-foundation modelling for vulnerability assessment of buildings in liquefied soils

M. D. L. Millen, J. Quintero, F. Panico, N. Pereira, X. Romão, A. Viana da Fonseca
CONSTRUCT, Faculty of Engineering, University of Porto, Porto, Portugal

ABSTRACT: Recent events have demonstrated that earthquake-induced liquefaction can result in significant structural damage and human casualties. The consideration of soil liquefaction has primarily been the domain of geotechnical engineering; however, recent studies have shown a strong interaction between liquefaction-development and the superstructure loads. Not only does liquefaction lead to a change in the shaking demands on the superstructure, it also changes the flexibility of the soil-foundation-structure system. Meanwhile, the high static shear forces from the foundation loads can result in a reduction or increase in pore pressure development. This strong soil-liquefaction-foundation-structure interaction (SLFSI) is a challenge for both geotechnical and structural engineers.

This paper develops an efficient numerical procedure for the vulnerability assessment of buildings with shallow foundations to the combined impacts of seismic shaking and liquefaction. The approach quantifies settlement and soil stiffness as time series to allow SLFSI to be considered in structural modelling in a simplified manner. The time series are developed through a combination of finite difference fully-coupled effective-stress modelling in FLAC and through analytical and empirical expressions based on key parameters. The framework is used to assess the vulnerability of a 3-storey reinforced concrete frame building to liquefaction and ground shaking.

1 INTRODUCTION

The dynamic seismic assessment of building performance and the consideration of impacts from soil liquefaction has often been considered completely separately. This separation is often done from necessity, because there are only a limited number of software packages that can suitably model the nonlinear structural elements and the coupled effective stress behaviour in the soil. In other cases the separation could be justified by the natural isolation effects that liquefaction causes, essentially limiting the seismic energy entering the building after liquefaction. However, liquefaction-induced seismic isolation does not always occur. In fact a weakened soil can amplify particular frequencies of a ground motion, thus increasing seismic demand, and field investigations summarised in Bird and Bommer (2004) after numerous earthquakes identified several cases where a combination of shaking and ground failure damage could be observed. Bird et al. (2006) discussed the issues with combining ground failure damage and shaking damage, and proposed a framework for estimating losses from combined damage, by first assessing structural performance to ground shaking and then assessing liquefaction demands using the residual capacity of the building and combining damage using a utility function based on the time of liquefaction. In fact the time of liquefaction has been recognised as a key parameter in understanding the contribution of shaking damage and liquefaction damage. Kramer et al. (2016) proposes a framework for estimating liquefaction-induced deformations that considered the time to liquefaction, where surface shaking and settlement rates may change once liquefaction occurs. Bouckovalas et al. (2017) uses a time to liquefaction based framework to estimate ground shaking demand by performing two site response analyses, one with pre-liquefaction properties and one with post-liquefaction properties.

One of the major impacts of liquefaction is in increased settlement, several recent research efforts (e.g. Negulescu and Foerster, 2010; Fotopoulou et al., 2018) have investigated the influence

of foundation differential settlement on structural damage by imposing ground deformation as a displacement to the end of a footing. Although this provides a conservative estimation of damage, in buildings greater than one storey this can lead to very large over estimation of damage as the stiffness of the frame acts to redistribute the gravity load on a settled footing into other footings thus reducing further settlement and increasing the settlement in other footings (Gómez-Martinez et al., 2018). In the proposed modelling approach, the issues of time of liquefaction, and of load redistribution, are considered in detail to better estimate the expected demands and deformations of the foundation and the building.

The modelling procedure developed in this paper is a sub-structuring approach and overcomes some of the issues of superposition by considering the rate of deformation rather than imposing displacements and forces. It has been developed to provide an efficient procedure to consider the impact of liquefaction on the performance of buildings for regional loss assessment (Viana da Fonseca et al., 2018). The model presented here is for the problem domain outlined in Figure 1, where the building is a Pre-1970's European reinforced concrete building on shallow foundations on flat ground, and subject to a ground motion only in one principle direction of the building. The development of the model requires four sub-steps:

1. Quantify the liquefaction potential of the soil profile in terms of depth and thickness of the liquefiable layer(s) and the resistance to liquefaction
2. Estimate the expected level of surface shaking considering the dynamic site response
3. Approximate the soil foundation stiffness using springs and dashpots that account for nonlinear soil behaviour and the change in soil characteristics due to liquefaction
4. Estimate the expected load-settlement behaviour of each footing accounting for the build up of pore pressure

The four sub-steps can either be performed separately on in combination. The following sections describe an approach to estimate the sub-steps using FLAC2D (ITASCA, 2017) and a series of simplified expressions.

The key aspects of the numerical model can be seen in Figure 1, where lumped plasticity is used to capture the nonlinear behaviour in the beams, columns, joints, infills and soil. Distributed gravity load is used to capture the expected static moment and shear demand on the elements. The input motion is the expected surface motion from sub step 2 and the expected differential settlement behaviour is captured through a combination of imposed settlement and changes in the stiffness of the soil springs. The full details of the numerical model are described in the following sections.

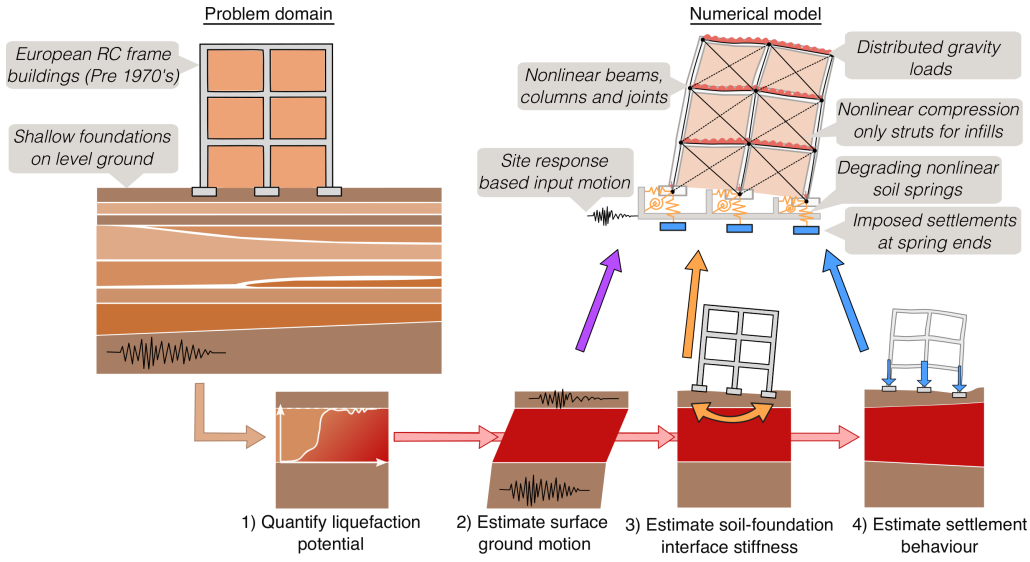

Figure 1.: Problem domain and numerical model

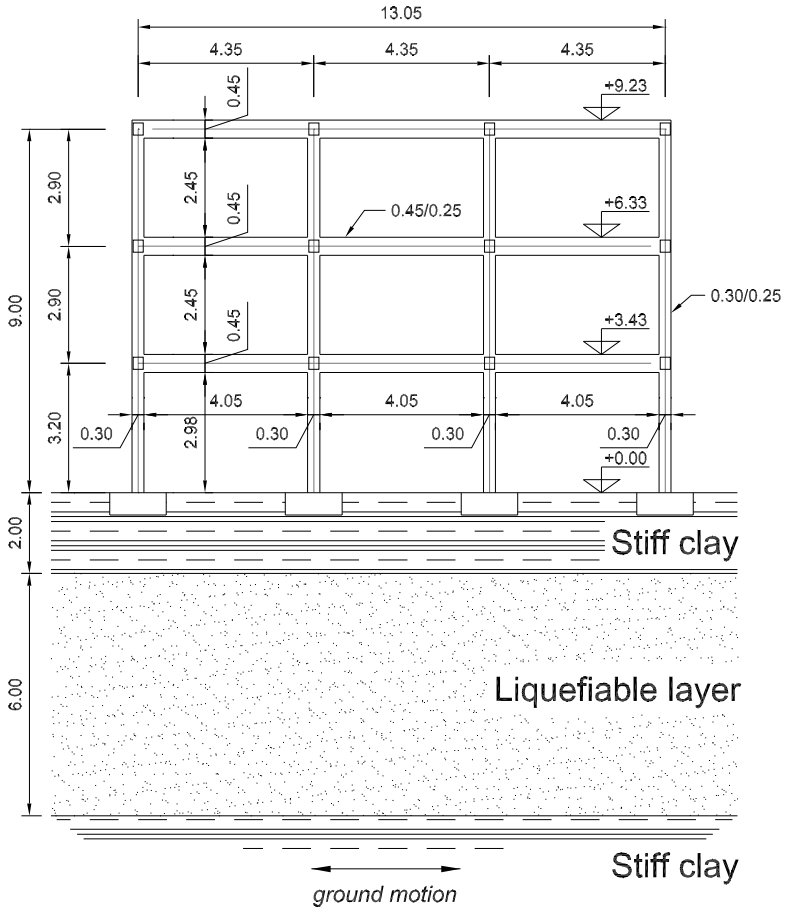

Figure 2.: Case study building and soil profile

2 CASE STUDY

The simple three-storey three-bay case study building and soil profile can be seen in Figure 2. The building had a first storey height of 3.2 m and other storeys of 2.9 m. The beams were 0.45 m deep and 0.25 m wide and the columns were 0.3 m deep and 0.25 m wide. The design concrete and steel strength were 16 MPa and 230 MPa respectively. The structural elements (beams, columns, joints, foundation footings) where all sized using a simulated design process, where the elements were designed to sustain the factored gravity loads on the beams of 50 kN/m. All columns have been designed with constant reinforcement with four 12 mm diameter rebars and 6 mm stirrups with a spacing of 0.15 m to give a column yield moment of 35 kNm. A specific reinforcement was designed for central and end sections of each beam. 16mm longitudinal rebars were used with 8mm stirrups in all the sections of all the beams. The yield moment of the beams was between 72 kNm and 156 kNm at the end sections. The footings were designed to be equal by considering the most loaded column and applying the Meyerhof (1963) method to design a squared section of 1.4 m with a depth of 0.55 m.

This procedure produced a non-seismic RC building. A second gravity analysis was then performed using a uniform load associated to the seismic combination of actions (15.5 kN/m on beams) and additional weight of the infills, in order to calculate the footing loads and nodal masses for the subsequent calculation of the settlement and the dynamic analyses.

The soil profile consisted of a top layer of 2 metre thick clay with a dry weight of 15.6 kN/m^3, undrained strength of 50 kPa, maximum shear modulus of 50 MPa, porosity of 0.412 and permeability of 8e-8 m/s. The 6 metre thick liquefiable sand had a saturated weight of 19.6 kN/m^3, constant volume friction angle ϕ=33 degrees, relative density Dr=65%, and permeability

k=1.6e-5 m/s. The liquefiable layer was also assigned the additional PM4Sand properties of normalised shear modulus of Go=782.7, and contraction rate parameter, hpo=0.32 (Boulanger and Ziotopoulou, 2017), for modelling in FLAC. The contraction rate parameter was calibrated by performing numerical element tests using the subroutines provided by the authors of the PM4Sand model and adjusting the parameter to obtain a cyclic resistance ratio of 0.15 for 15 cycles. The 12 metre thick clay on the bottom had a saturated weight 20.2 kN/m^3, undrained strength of 200 kPa, maximum shear modulus of 200 MPa, porosity of 0.375 and permeability of 1e-9 m/s. The ground water table was set at 2 m.

Only two ground motions were considered for the case study. The first motion was recorded at the Duzce station in Turkey with Vs30 of 280m/s, during the Kocaeli Earthquake 1999 (Mw=7.51) in Turkey, and the second from Dinar station with Vs30 of 220m/s, during the Dinar Earthquake 1995 (Mw=6.4) in Turkey, and were taken from the NGA2-west strong motion database from Ancheta et al. (2013) numbers 1158 and 1141 respectively. The two components for each record were rotated through 100 angles to obtained the maximum response in terms of Arias Intensity.

Given the simplistic of the model and the large variation that could be expected in the soil, structural and ground motion properties, suitable variation in modelling assumptions, and parametric variations should be considered when modelling a real building, however, for the purposes of this paper a deterministic approach was more suitable for illustrating the modelling techniques.

3 ESTIMATING THE INPUTS FOR NUMERICAL MODEL

3.1 *Estimating liquefaction potential and surface shaking*

The liquefaction potential has already been described in terms of a cyclic resistance ratio for 15 uniform cycles and the depth and thickness of the layer, however, the settlement and stiffness estimations require a time series of pore pressure build up. The ground surface motion is also required and therefore a 1D fully coupled effective stress analysis of the soil profile was performed in FLAC 2D (ITASCA, 2017). The selected ground motions were input as a stress at the base of the model without deconvolution since the real soil profile that they were recorded on was unknown. Therefore the analyses rely on the assumption that any strong stiffness stratification that would result in significant reflection of seismic waves was sufficiently deep that the ground motion characteristics of the upward propagating motion at 20m depth would be similar to half of the surface motion. The PM4Sand model was used to simulate the liquefiable soil layer and the clay layers were modelled with the Mohr-Coulomb model and hysteretic damping consistent with the shear modulus reduction curve (Vardanega and Bolton, 2013) for plastic index of 30%. An additional 2.0% Rayleigh damping was set at 0.65 Hz (approximate site period) and 5 Hz.

The results of the 1D analysis can be seen in Figure 3 where in both motions liquefaction occurs at near 10 seconds based on the pore pressure ratio (r_u) plots reaching values close to one. The pore pressure builds up more rapidly in the first motion and then surface shaking reduces to a negligible level, while for the second motion the surface acceleration exhibits some acceleration peaks as the base motion remains strong and the soil dilates. The peaks are largely high frequency content as can be observed in the Stockwell transform. The surface motions were filtered at 15 Hz before being used in the structural analysis to improve analysis speed and because some amplification occurred at high frequencies due to numerical noise when liquefaction occurred, consistent with Tsiapas and Bouckovalas (2018).

3.2 *Estimating the soil-foundation interface stiffness*

The soil-foundation impedance was model using a single spring and dashpot for each of the vertical, horizontal and rotational degrees-of-freedom for each footing and the initial properties were determined using the formulations proposed in Gazetas (1991). The dynamic coefficients were taken as 1, except for the rotational dashpot, where the dynamic co-efficent was calculated as 0.1 from Gazetas (1991).

The horizontal stiffness was modelled as constant linear elastic, while the vertical and rotational springs were degraded based on the build up of pore pressure. The vertical stiffness was modelled as a linear no-tension spring using the elastic no-tension material (ENT material) in Opensees. The spring stiffness decreased linearly with an increase in the pore pressure ratio r_u from an initial value $K_{v,i}$ corresponding to $r_u = 0$ to a residual value $K_{v,res}$ at $r_u = 1$, where the degraded value

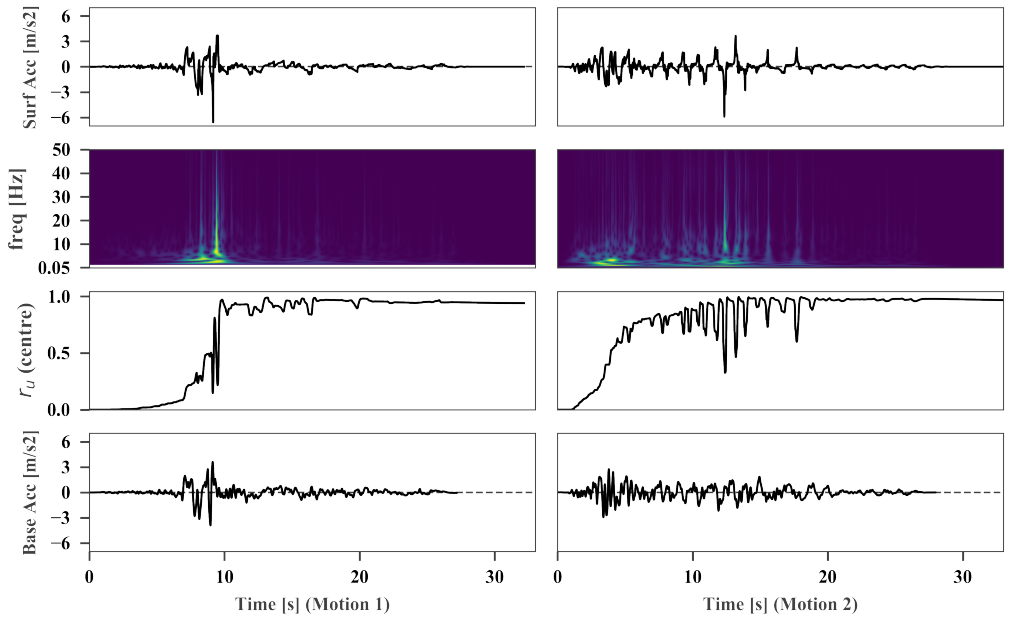

Figure 3.: Results from 1D effective stress analyses

was calculated based on Karatzia et al. (2017) and a shear wave velocity for the liquefied soil of 30m/s. The stiffness was calculated at each step by reading in the r_u time series from the centre of the liquefiable layer from the FLAC output. The change in the vertical stiffness was not intended to capture the liquefaction-induced settlement (which was modelled through vertical displacements at the spring ends and is typically driven by many mechanisms as well as vertical loading) as the spring deformation in the case study was less than 2 mm. However, the vertical resistance of the soil can be a crucial parameter in the redistribution of loads and in the change of the dynamic response period of the soil-foundation-structure system. The rotational spring was both deformation and pore pressure dependent and was modelled in Opensees using material PyLiq1 from Boulanger et al. (1999). Here the ultimate rotation capacity was input for the non-liquefied soil calculated using Equation 1. Where B is the footing width, N is the static vertical load, and N_{cap} is the foundation bearing capacity in static conditions. The residual moment capacity was calculated by using the ratio from Karatzia et al. (2017) for the rotational stiffness, and the pore pressure time series from FLAC was used to reduce the capacity. The rotational damping was modelled within the PyLiq1 element by setting the equivalent dashpot coefficent, whereas the damping for the other modes was modelled with the Opensees dashpot elements in parallel with the springs.

$$M_{cap,i} = M_y = N\frac{B}{2}\left(1 - \frac{N}{N_{cap}}\right) \tag{1}$$

3.3 *Estimating the foundation load-settlement behaviour*

The seismically-induced dynamic settlement (S) was estimated through an adapted version of the simplified settlement model (Equation 2) by Karamitros et al. (2013), where CAD is the cumulative absolute displacement or integral of the velocity time series, Z_{liq} is the height of the liquefiable layer, and FS_{deg} is the degraded bearing capacity factor of safety calculated according to Karamitros et al. (2013). The first adaption approximated the settlement as a time series by using the CAD and weighted by the pore pressure, such that it would give the same final displacement (Equation 3). The second adaption was to consider that the vertical load changes through out the time series due to frame-action and load redistribution from differential settlement. The degraded bearing capacity was kept the same as from Karamitros et al. (2013) as the degradation was already partially considered through the weighting factor based on the pore pressure, but the

vertical load on the footing was taken from Opensees at each time step to recompute the factor of safety and the expected change in displacement. Equation 3 was therefore modified to consider the differential of the settlement with respect to CAD, and then the change in CAD, the pore pressure ratio and the vertical load were used to calculate the expected change in settlement over a time step. While these adaptions allow for the consideration of load redistribution and settlement during a seismic event, the adaptions have not been calibrated and were made in a way to best reflect the original work by Karamitros et al. (2013).

$$S = CAD \cdot (Z_{liq})^{1.5} \left(\frac{1}{FS_{deg}} \right)^3 \tag{2}$$

$$S_i = \frac{\sum_0^i |v_i| \cdot r_{u,i}}{\sum_0^n |v_i| \cdot r_{u,i}} \cdot CAD \cdot (Z_{liq})^{1.5} \left(\frac{1}{FS_{deg}} \right)^3 \tag{3}$$

In order to model the differential settlement due to soil non-homogeneity, two sets of analyses were run: in the first, the formulation presented above was directly applied. In the second set, the rate was adjust for each footing by a random coefficient (1.107, 1.153, 0.763, 1.157 for footings from F1 to F4, respectively).

3.4 *Structural model*

The building was modelled using elastic beam and column elements with nonlinear plastic hinges, joints and infills in OpenSees (Figure 4). The gravity load for seismic combination of actions was applied as a distributed load along beams and additional infill mass at the nodes. A simple leaning column model was used to account for additional gravity in the design building to capture the P-delta effects (not shown in the figure). The ground motion was applied at the ends of the horizontal springs and the imposed settlements at the bottom ends of the vertical spring elements. The beam-column joint element (Joint2D element) was idealised as a parallelogram shaped shear panel (rotational spring) with adjacent elements connected to its mid-points. Each beam or column was connected to the shear panel through a shear and a rotational spring (ZeroLength elements). The system composed by the shear panel and the four spring elements at the external nodes is able to reproduce the nonlinear response of the structure under monotonic and cyclic strain, thanks to the materials associated to each component. The central rotational spring was modelled with a hysteretic material (uniaxialMaterial Hysteretic), with pinching of force and deformation, damage due to ductility and energy, and degraded unloading stiffness based on ductility. The external rotational springs were modelled with a material (ModIMKPeakOriented) that simulates the modified Ibarra-Medina-Krawinkler deterioration model with peak-oriented hysteretic response (Lignos and Krawinkler, 2012). The strength and stiffness associated to these materials was a function of the physical characteristics of the sections of the corresponding elements (beams or columns), that were determined in the design phase, where the reinforcement characteristics were determined.

The masonry infills were modelled with the equivalent strut approach, using diagonal nonlinear truss elements with the Concrete01 material. Two diagonal struts were used to simulate one infill and were connected to the beam-column joints (at the column node) (Figure 4). The equivalent area and compressive stress of each strut was established using (Žarnić and Gostič, 1997) based on the maximum lateral force of the infill assuming an effective thickness of 0.1 m, and then transformed to the direction of the diagonal. Maximum strength was calculated as 144 kN and 135 kN for the first and upper floors respectively and was assumed to be reached at an inter-storey drift of 0.2% based on (Dolšek and Fajfar, 2008), a residual stress equal to 10% of the maximum stress is considered for numerical stability, which is reached at an inter-storey drift five times the inter-storey drift at maximum strength. The lateral displacement of each infill was transformed into the diagonal displacement for the subsequent definition of the strain of the strut.

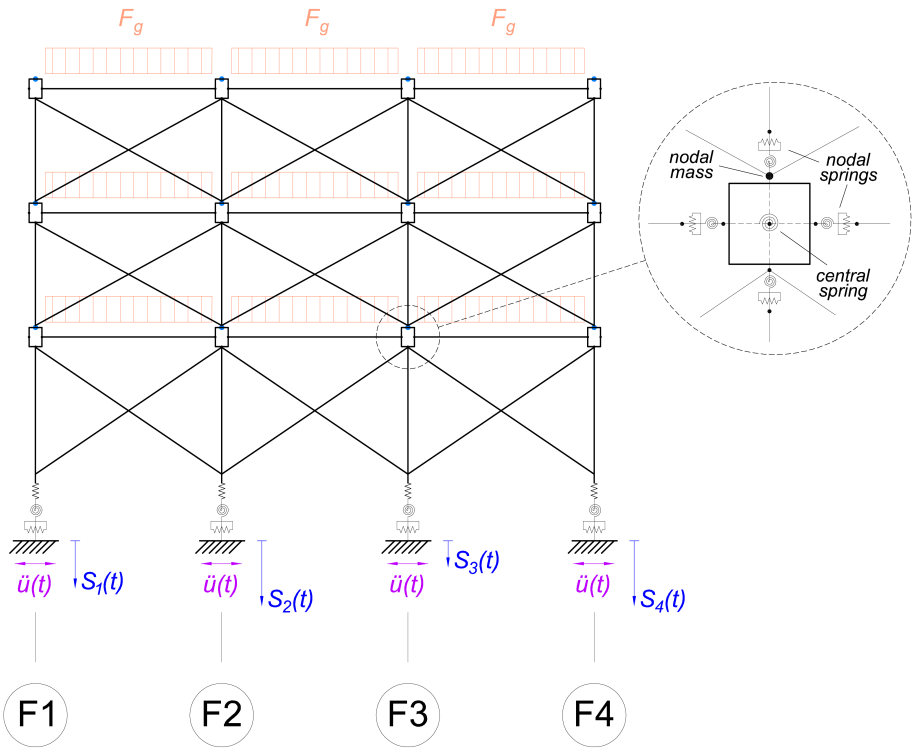

Figure 4.: Numerical model and detail of the beam-column joints configuration

3.5 *Results*

The results presented here consider the structural model with and without infills; and with the settlement increments applied with the same intensity and with the application of random coefficients. Each set of analyses were performed with the two ground motions (one for each analysis) described in the precedent sections.

The results for the analyses performed with uniform settlement coefficients are reported in Figure 5. In the case of the structure without infills (Figure 5 a & e), a soft-storey is created at the ground floor; in fact, the maximum value of inter-storey drift θ_1 is approximately equal to 3% for the first motion and 4% for the second motion (blue dots in figure), much higher than the drifts of the upper floors and the foundation tilt ($<$1%). Thus, the distortion is located in the columns of the ground floor, which during and after the shaking are not perpendicular to the foundation plane and to the beams of the first floor.

The flexibility of the structure is visible in the settlement of the footings, which were higher for the central footings (F2 and F3), and smaller for the external footings (F1 and F4). This is expected as using the initial vertical loads and Equation 3 would result in almost 8 times the settlement in the central footings compared to the outer footings, due to the larger tributary area and consequent vertical on the central footings (dashed lines in Figure 5 c, d, g, h). However, the difference in settlement between the footings is not very large. This is the effect of load redistribution: central footings, which initially take the higher share of the gravity load are subjected to a higher settlement than the external footings. This causes the vertical load to be transferred from the central to the external footings, until the load is approximately equally shared among the four pads. The settlement was nearly equal for the two central footings and for the two external footings and almost no global tilt was observed. The average settlement simulated here by accounting for load re-distribution is approximately double the settlement calculated with Equation 3 as seen in Figures 5c, d, g and h. This increase in settlement can be attributed to the additional frame action due to seismic loading on the structure, and therefore produces cyclic vertical load on the footings, in some instances more than double the static load. While the settlement equation from Karamitros et al. (2013) was only developed for shear loading of the soil and did not consider the influence of frame-action, this simple adaption appears to provide reasonable estimates of

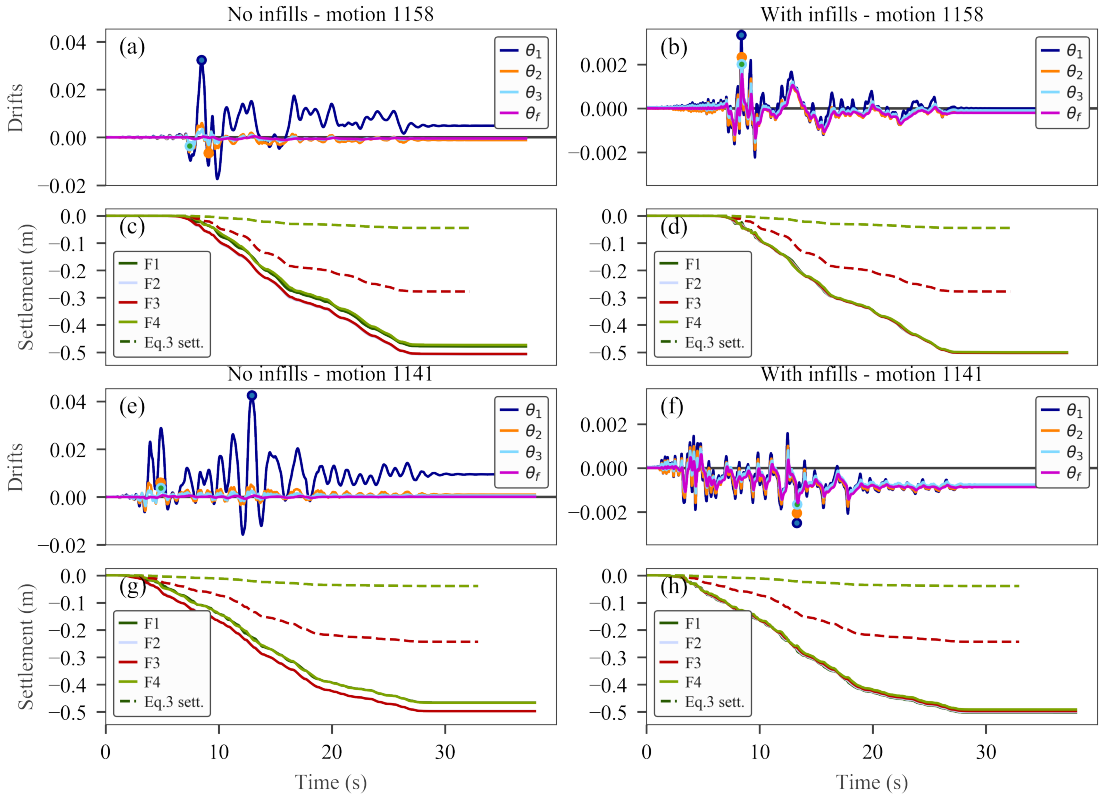

Figure 5.: Drift and settlement results with equal incremental settlement analyses, a&c) motion 1158 no infills, b&d) motion 1158 with infills e&g) motion 1141 no infills f&h) motion 1141 no infills

behaviour and exhibiting similar mechanisms to those observed by Luque and Bray (2017) using advanced effective stress analyses.

The analyses performed considering the structure equipped with the infills shows a clearly more rigid structure with respect to the precedent (no infills) case (Figure 5 b & f). The inter-storey drifts and the foundation tilt are in phase and present similar values. The maximum values were less than 0.3%, ten times less than in the no infills case. The coherent response of the inter-storey drifts and foundation tilt produces rigid movements of the structure rather than angular distortions between structural elements. The average footing settlement was around 0.5 m, the same as for the no infills case, but the rigidity of the superstructure made the settlements equal for all the footings. The analysis performed with ground motion GM2 shows a small residual foundation tilt (around 0.1%).

The results of the analyses performed imposing random coefficient to the incremental settlements are shown in Figure 6 for only ground motion one (ID 1158), as the second ground motion produced the same conclusions. For each analysis, the drifts of the superstructure were very similar to the corresponding drifts of the precedent case where the settlements were applied with no scaling coefficient. The foundation tilt in this case was not nil, being approximately equal to 0.2% in the negative (counter clockwise) direction. The distortion of the ground floor in the case of structure without infills was aggravated by the foundation tilt (which was in the opposite direction). As for the structure with infills, the rigid rotation of the foundation plane was associated with a congruent rotation of the superstructure, which tilted without major distortion between the structural elements.

As expected, the settlements of the four footings shows a higher dispersion than in the case where the settlements were applied with no random scaling coefficient. It is interesting to note that the tilt of the foundation plane was in all cases in the counter clockwise direction, although the settlement coefficient of footing F1 was lower than the coefficient of F4, which would suggest a rotation in the opposite sense. Nevertheless, examining the vertical load on the footings at

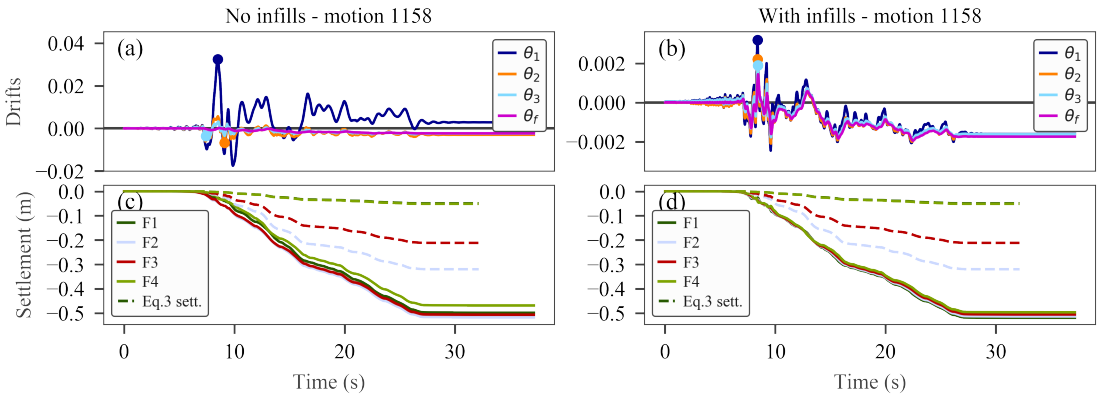

Figure 6.: Drift and settlement results with random factors applied to incremental settlements a&c) motion 1158 no infills, b&d) motion 1158 with infills

the end of shaking, footing F3 was the most loaded, followed by F1, F2, and F4, respectively. This reflects the order of the random coefficients from the minimum to the maximum. Since the superstructure was very rigid compared to the soil (with or without infills), its vertical reaction was governed by the two more loaded (i.e. prone to less settlement) footings, F3 and F1. Footings F2 and F4 had a higher allowable settlement rate, thus, their load was progressively redistributed by the superstructure to footings F1 and F3. If the foundation tilt is calculated between F1 and F3, a negative value (i.e. in the counter clockwise direction) is obtained. This reflects the fact that the coefficient associated to F3 is lower than the coefficient associated to F1.

The dashed lines in Figure 6 a & d, represent the settlement time series for the four footings calculated with Equation 3, scaled with the four constant random coefficients reported earlier. The dashed lines present a higher dispersion than the footing settlements from the analyses. Again this is due to the load redistribution from the more loaded springs to the less loaded, and the consequent change in the factor of safety.

4 CONCLUSIONS

The framework and procedure presented in this paper offers a numerically efficient approach for engineers to considering the impacts of liquefaction on buildings. Although some of the inputs (e.g. rate of settlement) are not yet well calibrated, the efficiency of the procedure and the decoupling of the liquefaction analysis and structural analysis, allows engineers to consider a variation of the material properties and of underlying assumptions to obtain the inputs for the structural analysis. The case study building that was investigated using the presented procedure did not suffer from large differential settlement and the infills provided significant additional capacity to resist differential settlements and inter-storey drifts. In light of these findings further understanding of the performance of infills to combine loading from seismic and differential settlement may be warranted as well as further research into the modification of seismic shaking, settlement rate and soil-foundation impedance due to liquefaction.

5 ACKNOWLEDGEMENTS

This paper was produced as part of the LIQUEFACT project (Assessment and mitigation of liquefaction potential across Europe: a holistic approach to protect structures/infrastructures for improved resilience to earthquake-induced liquefaction disasters) has received funding from the European Union's Horizon 2020 research and innovation programme under grant agreement No GAP-700748.

REFERENCES

Ancheta, T. D., R. Darragh, J. P. Stewart, S. Emel, W. Silva, B. Chiou, K. E. Wooddell, R. W. Graves, A. R. Kottke, D. M. Boore, T. Kishida, & J. Donahue (2013). PEER NGA-West2 Database. Technical Report 03, USA.

Bird, J. F. & J. J. Bommer (2004). Earthquake losses due to ground failure. *Engineering Geology 75*(2), 147–179.

Bird, J. F., J. J. Bommer, H. Crowley, & R. Pinho (2006). Modelling liquefaction-induced building damage in earthquake loss estimation. *Soil Dynamics and Earthquake Engineering 26*(1), 15–30.

Bouckovalas, G. D., Y. Z. Tsiapas, V. A. Zontanou, & C. G. Kalogeraki (2017). Equivalent Linear Computation of Response Spectra for Liquefiable Sites: The Spectral Envelope Method. *Journal of Geotechnical and Geoenvironmental Engineering 143*(4), 04016115–12.

Boulanger, R. W., C. J. Curras, B. L. Kutter, D. W. Wilson, & A. Abghari (1999). Seismic soil-pile-structure interaction experiments and analyses. *Journal of Geotechnical and Geoenvironmental Engineering 125*(9), 750–759.

Boulanger, R. W. & K. Ziotopoulou (2017). PM4SAND (Version 3.1): A Sand Plasticity Model for Earthquake Engineering Applications. pp. 1–113.

Dolšek, M. & P. Fajfar (2008). The effect of masonry infills on the seismic response of a four-storey reinforced concrete framea deterministic assessment. *Engineering Structures 30*(7), 1991–2001.

Fotopoulou, S., S. Karafagka, & K. Pitilakis (2018). Vulnerability assessment of low-code reinforced concrete frame buildings subjected to liquefaction-induced differential displacements. *Soil Dynamics and Earthquake Engineering 110*, 173–184.

Gazetas, G. (1991). Foundation vibrations. In *Foundation engineering handbook*, pp. 553–593. Springer.

Gómez-Martinez, F., M. D. L. Millen, P. A. Costa, X. Romão, & A. Viana da Fonseca (2018). Potential Relevance of Differential Settlements in Earthquake-induced Liquefaction Damage Assessment. In *16th European Conference on Earthquake Engineering*, Thessaloniki.

ITASCA (2017). FLAC2D - Fast Lagrangian Analysis of Continua, Version. 8.0. Minneapolis: Itasca.

Karamitros, D. K., G. D. Bouckovalas, & Y. K. Chaloulos (2013). Seismic settlements of shallow foundations on liquefiable soil with a clay crust. *46*(C), 64–76.

Karatzia, X., G. Mylonakis, & G. Bouckovalas (2017). Equivalent-linear dynamic stiffness of surface footings on liquefiable soil. In *COMPDYN 2017 - Proceedings of the 6th International Conference on Computational Methods in Structural Dynamics and Earthquake Engineering*, pp. 1388–1402. National Technical University of Athens.

Kramer, S. L., S. S. Sideras, & M. W. Greenfield (2016). The timing of liquefaction and its utility in liquefaction hazard evaluation. *Soil Dynamics and Earthquake Engineering 91*(C), 133–146.

Lignos, D. G. & H. Krawinkler (2012). Development and utilization of structural component databases for performance-based earthquake engineering. *Journal of Structural Engineering 139*(8), 1382–1394.

Luque, R. & J. D. Bray (2017). Dynamic Analyses of Two Buildings Founded on Liquefiable Soils during the Canterbury Earthquake Sequence. *143*(9), 04017067–04017014.

Meyerhof, G. G. (1963). Some recent research on the bearing capacity of foundations. *Canadian Geotechnical Journal 1*(1), 16–26.

Negulescu, C. & E. Foerster (2010). Parametric studies and quantitative assessment of the vulnerability of a RC frame building exposed to differential settlements. *Natural Hazards and Earth System Science 10*(9), 1781–1792.

Tsiapas, Y. Z. & G. D. Bouckovalas (2018). Numerical noise effects and filtering in liquefiable site response analyses. In *Numerical Methods in Geo Eng IX*, pp. 1–8.

Vardanega, P. J. & M. D. Bolton (2013). Stiffness of Clays and Silts: Normalizing Shear Modulus and Shear Strain. *Journal of Geotech. and Geoenv. Engineering 139*(9), 1575–1589.

Viana da Fonseca et al., A. (2018). Methodology for the liquefaction fragility analysis of critical structures and infrastructures: description and case studies. *LIQUEFACT Deliverable 3.2. Horizon 2020 European Union funding for Research and Innovation Project ID: 700748 (www.liquefact.eu)*.

Žarnić, R. & S. Gostič (1997). *Masonry infilled frames as an effective structural sub-assemblage*.